Probability distribution for energy of saturated broadband ocean acoustic transmission: Results from Gulf of Maine 2006 experiment

Duong Tran, Mark Andrews, and Purnima Ratilal[a)]
Department of Electrical and Computer Engineering, Northeastern University, 360 Huntington Avenue, Boston, Massachusetts 02115

(Received 4 November 2011; revised 4 September 2012; accepted 28 September 2012)

The probability distribution of ocean-acoustic broadband signal energy after saturated multipath propagation is derived using coherence theory. The frequency components obtained from Fourier decomposition of a broadband signal are *each* assumed to be fully saturated with energy spectral density that obey the exponential distribution with 5.6 dB standard deviation and unity scintillation index. When the signal bandwidth and measurement time are larger than the correlation bandwidth and correlation time, respectively, of its energy spectral density components, the broadband signal energy obtained by integrating the energy spectral density across the signal bandwidth then follows the Gamma distribution with a standard deviation smaller than 5.6 dB and a scintillation index less than unity. The theory is verified with broadband transmissions in the Gulf of Maine shallow water waveguide in the 300 to 1200 Hz frequency range. The standard deviations of received broadband signal energies range from 2.7 to 4.6 dB for effective bandwidths up to 42 Hz, while the standard deviations of individual energy spectral density components are roughly 5.6 dB. The energy spectral density correlation bandwidths of the received broadband signals are found to be larger for signals with higher center frequencies and are roughly 10% of each center frequency.
 [http://dx.doi.org/10.1121/1.4763547]

PACS number(s): 43.30.Bp, 43.30.Re [AMT] Pages: 3659–3672

I. INTRODUCTION

The probability density functions for the energy spectral density[1] and total energy of a broadband signal transmitted through an ocean-acoustic waveguide are derived using fourth-order coherence theory.[1–4] The probability distributions are formulated in terms of the signal bandwidth, measurement time, frequency, and temporal correlation of the broadband signal's energy spectral density components. The statistical theory is verified with data from the Gulf of Maine 2006 Experiment (GOME'06)[5,6] where broadband acoustic transmissions in the 300 to 1200 Hz frequency range and effective bandwidths up to 42 Hz were measured at source-receiver separations of up to 20 km.

When an acoustic field propagates through a temporally random and spatially inhomogeneous ocean waveguide, its intensity or energy fluctuates in both time and space. In both deep ocean and shallow water continental shelf environments, a major source of acoustic field scintillation is internal waves.[7–9] Early efforts to describe signal scintillation statistics in the ocean were based on multipath theory, with the resultant field being the sum of multiple random phase components.[10–12] The instantaneous received signal therefore has an exponential distribution for intensity or a Rayleigh distribution for amplitude,[10–12] and a 5.6 dB intensity standard deviation.[11] The formulations in Refs. 10–12 assume a uniform distribution for instantaneous phase at saturation due to multipath effects. In a later study,[2] statistics of acoustic signals were characterized as a function of measurement time T and intensity correlation time τ_c, where a time-averaged measurement of signal intensity was shown to be equivalent to a measurement of instantaneous intensity contributions from μ_T independent and identically distributed fluctuating sources or correlation cells. The time-averaged signal intensity therefore has a Gamma distribution[1,2,13,14] and a standard deviation less than 5.6 dB. Here we derive the probability distributions for the bandwidth-integrated energy of a broadband signal and its corresponding time-averaged quantity by applying coherence theory, which characterizes the coherence or correlation properties of a wave field through second or higher-order correlation functions.[1–4] The derivation in the current paper generalizes and extends the statistical theory of Ref. 2 since it includes the frequency correlation of broadband signals not considered in that reference. We show that the total number of independent statistical fluctuations or correlation cells[1,2] μ can be increased for a broadband signal by extending either or both the signal bandwidth and measurement time.

The energy spectral density components as a function of frequency of the received broadband signals in the Gulf of Maine were found to have standard deviations of approximately 5.6 dB and scintillation indices (SIs) that approach 1, which are characteristics of a saturated field. The energy spectral density components of the measured data fit well with the exponential distribution based on a two-sided chi-squared test. The broadband signal energies obtained by integrating the energy spectral densities over the signal

a)Author to whom correspondence should be addressed. Electronic mail: purnima@ece.neu.edu

bandwidths were found to have smaller standard deviations ranging from 2.7 to 4.6 dB and SIs significantly smaller than 1 for signals with effective bandwidths of up to 42 Hz. The broadband signal energies were found to follow the Gamma distribution and depart significantly from the exponential distribution when the total number of frequency correlation cells of the broadband signal exceeded 2. Smaller standard deviations and SIs were associated with a larger bandwidth and smaller center frequency signals. The measured broadband signal contains saturated frequency components but decorrelation across its bandwidth after forward propagation and scattering in a random ocean waveguide leads to one or more independent frequency fluctuations or frequency correlation cells, thereby reducing the broadband signal's energy standard deviation. The energy spectral density correlation bandwidth of the measured broadband signals is found to be roughly 10% of the center frequency. The measurements of broadband signal energy standard deviations in other shallow water waveguides are consistent with the statistical theory presented here[15,16] as discussed in Sec. III G.

Previous experimental and theoretical studies of ocean acoustic transmission scintillation in shallow and deep ocean environments have examined a variety of quantities including intensity and arrival time of individual rays or modes, pulse time spreads, phase, and energy distributions.[7,15,17,18] Several of these experiments employed *vertical* receiving arrays at fixed locations from a source to analyze the statistics of individual ray or modal arrivals from the depth-dependent received fields.[15,18,19] Many deep ocean acoustic transmission experiments found the acoustic field to be partially saturated with a significant mean field contributing to the total intensity or energy.[17,20] The acoustic transmission data from shallow water, on the other hand, were often found to be saturated with a negligible mean field at sufficiently large ranges from the source.[15,16] The theory developed here is applicable for analyzing broadband acoustic propagation at ranges beyond roughly 3 km in typical continental shelf environments since the received field is expected to be saturated.[15,16]

Here, we focus our analysis on the statistics of the energy spectral density and total energy of the broadband acoustic transmissions in the Gulf of Maine shallow water waveguide with measurements made on a single hydrophone. The received field on the hydrophone is a sum of multi-modal contributions that involve significant bottom interaction along the propagation path as will be shown in Sec. III A which leads to a received field that is saturated. The energy of a broadband signal is an important quantity often used to infer parameters such as target strength or scattering strength of objects in active sensing,[5,6,21–23] digital logic levels of transmitted messages in underwater acoustic communication systems,[24,25] and the level of underwater broadband sources, such as vocalizing marine mammals[26–28] and underwater vehicles. An understanding of the statistics of broadband signal energy and its dependence on signal bandwidth, center frequency, and measurement time is necessary to efficiently design experiments, and to quantify the accuracies with which the related parameters can be determined.

II. PROBABILITY DISTRIBUTION FOR SATURATED BROADBAND SIGNAL ENERGY AS A FUNCTION OF SIGNAL BANDWIDTH, MEASUREMENT TIME, FREQUENCY CORRELATION, AND TEMPORAL CORRELATION

A. Probability distribution for the energy of a broadband signal with measurement time smaller than energy spectral density correlation time

Here we derive the probability density function for the energy of a broadband signal in terms of its physical bandwidth B and the frequency correlation width B_c of its energy spectral density components. This derivation parallels that given in Refs. 1 and 2 where the probability distribution of time-averaged intensity is formulated in terms of a signal's measurement time T and the correlation time τ_c of its instantaneous intensity measurements. The correlation time[1,2] refers to the characteristic time period of fluctuation of the random acoustic field. It can be derived by considering the fourth-order temporal coherence[1] of the underlying complex field [see Eqs. (A8) and (31)]. Here, we first consider the scenario where the measurement time is smaller than the energy spectral density correlation time $(T < \tau_c)$, so that the broadband signal has only one temporal correlation cell $\mu_T = 1$.

Let the received broadband signal in time with bandwidth B and center frequency f_m be denoted by $\psi(t)$. We assume that the broadband signal duration T_D is much smaller than its correlation time $(T_D \ll \tau_c)$. This is a reasonable assumption since the broadband signals transmitted in the ocean typically have durations on the order of seconds,[5,21] while the correlation time scale of signal fluctuation is much larger, on the order of several to tens of minutes.[18,29,30] We also assume the observation or measurement time T satisfies $T > T_D$ and $T < \tau_c$. The complex spectral amplitude $\Phi(f|t_k)$ of the signal can be obtained by Fourier analysis

$$\Phi(f|t_k) = \int_{t_k}^{t_k+T_D} \Psi(t) e^{j2\pi ft} dt, \tag{1}$$

where t_k is the time instance when the signal first arrives at the receiver. For a saturated broadband signal, its Fourier components $\Phi(f|t_k)e^{-j2\pi ft}$ each have an envelope $\Phi(f|t_k)$ that can be modeled as a circular complex Gaussian random variable. At saturation, the real and imaginary parts of $\Phi(f|t_k)$ are independent Gaussian random variables with zero mean and the same variance.[2,11] Since $T_D \ll \tau_c$, the Fourier complex amplitude $\Phi(f|t_k)$ can be approximated as instantaneous in time.

The energy spectral density $\mathcal{E}(f|t_k)$ obtained from magnitude-squared amplitude of a Fourier component

$$\mathcal{E}(f|t_k) = |\Phi(f|t_k)|^2, \tag{2}$$

obeys the exponential distribution

$$p(\mathcal{E}) = \begin{cases} \frac{1}{\bar{\mathcal{E}}} \exp[-\mathcal{E}/\bar{\mathcal{E}}], & \text{for } \mathcal{E} \geq 0, \\ 0, & \text{elsewhere,} \end{cases} \tag{3}$$

with mean and standard deviation both equal to $\bar{\mathcal{E}}$. The phase of $\Phi(f|t_k)$ is uniformly distributed over 2π radians for the saturated signal.

The bandwidth-averaged energy spectral density $\mathcal{J}(f_m|t_k, B)$ is

$$\mathcal{J}(f_m|t_k,B) = \frac{1}{B}\int_{f_m-B/2}^{f_m+B/2} \mathcal{E}(f|t_k)df = \frac{1}{B}\int_{t_k}^{t_k+T_D} |\Psi(t)|^2 dt \quad , \tag{4}$$

where the last equality is obtained by application of Parseval's theorem. The mean and variance of $\mathcal{J}(f_m|t_k, B)$ are derived in Appendix A and given by Eqs. (A1) and (A14), respectively. A measure of the number of independent spectral fluctuations or frequency correlation cells μ_F averaged over bandwidth B is given by the squared-mean-to-variance ratio or signal-to-noise ratio[1,2] of the measurement $\mathcal{J}$

$$\mu_F(f_m) = \frac{\langle \mathcal{J}(f_m|t_k, B)\rangle^2}{\langle \mathcal{J}^2(f_m|t_k, B)\rangle - \langle \mathcal{J}(f_m|t_k, B)\rangle^2} = \left[\frac{1}{B}\int_{-\infty}^{\infty} \Delta\left(\frac{\xi}{B}\right)\rho(\xi, \tau = 0|f_m)d\xi\right]^{-1}, \tag{5}$$

where $\rho(\xi, \tau|f_m)$ is the joint temporal-spectral correlation coefficient of the energy spectral density components of the broadband signal defined in Eq. (A11), and the triangular function $\Delta(\xi/B)$ is defined in Eq. (A10) of Appendix A. The energy spectral density undergoes fluctuations over a characteristic bandwidth B_c that is referred to as its frequency correlation width. A useful measure of the correlation bandwidth of the energy spectral density of the broadband signal centered at frequency f_m is then given by

$$B_c(f_m) = \int_{-\infty}^{\infty} \rho(\xi, \tau = 0|f_m)d\xi. \tag{6}$$

Another measure of the correlation bandwidth $B_c(f_m)$ is twice the e-folding frequency shift ξ_e satisfying $\rho(\xi_e, \tau = 0|f_m) = 1/e$.

The physical meaning of the number of frequency correlation cells μ_F can be understood by considering its limiting values. For a small bandwidth signal $B \ll B_c$, the energy spectral density across the signal's physical bandwidth B can be considered perfectly correlated, so that $\rho(\xi, \tau = 0|f_m) \approx 1$ for $-B/2 \le \xi \le B/2$. Equation (5) can then be approximated as $\mu_F = B[\int_{-\infty}^{\infty} \Delta(\xi/B)d\xi]^{-1} = 1$. This result may be interpreted as that when the bandwidth shrinks, the number of frequency correlation intervals influencing the experimental measure asymptotically approaches unity. Values of μ_F less than unity are not possible because the results are always influenced by the state of the field in at least one correlation cell.[1] For a large bandwidth signal, $B \gg B_c$, since the width of the triangular function is $2B$ and the width of the frequency correlation coefficient is roughly B_c, Eq. (5) can be approximated as $\mu_F = B[\int_{-\infty}^{\infty} \rho(\xi, \tau = 0|f_m)d\xi]^{-1} = B/B_c$. The number of frequency correlation intervals contained within the physical bandwidth B in this case can be obtained by dividing B by the correlation bandwidth B_c. These values for the number of frequency correlation cells μ_F are obtained in direct analogy to Eqs. (6.1-17) and (6.1-19) of Ref. 1, which are expressed for the number of temporal correlation cells. This implies that more accurate experimental estimates of the correlation bandwidth can only be obtained from received broadband signals with large physical bandwidths.

Since the bandwidth-averaged energy spectral density $\mathcal{J}(f_m|t_k, B)$ of the broadband signal can be decomposed into the sum of μ_F independent exponentially distributed spectral fluctuations, its probability density function is then described by the Gamma distribution[1,2] with shape parameter μ_F and scale parameter $\bar{\mathcal{E}}/\mu_F$

$$p(\mathcal{J}) = \begin{cases} \frac{1}{\Gamma(\mu_F)}\left(\frac{\mu_F}{\bar{\mathcal{E}}}\right)^{\mu_F} \mathcal{J}^{(\mu_F-1)}\exp\left(-\mu_F\frac{\mathcal{J}}{\bar{\mathcal{E}}}\right), & \text{for } \mathcal{J} \ge 0 \\ 0, & \text{elsewhere.} \end{cases} \tag{7}$$

The above equation is readily obtained from the inverse Fourier transform of the characteristic function[1,13] or moment generating function of the exponential distribution raised to the power μ_F. To obtain Eq. (7), we have assumed that the mean of the energy spectral density $\bar{\mathcal{E}}$ is approximately constant for the frequency components across the signal bandwidth B. We will show that this is a valid assumption for the signals considered here in Sec. III C. Compared to the exponentially distributed energy spectral density of a monochromatic component $\mathcal{E}(f|t_k)$, the expected value of the Gamma distributed bandwidth-averaged energy spectral density $\mathcal{J}(f_m|t_k)$ is still $\bar{\mathcal{E}}$ but the variance is modified to $\bar{\mathcal{E}}^2/\mu_F$ (see Appendix A). When $\mu_F > 1$ the bandwidth-averaged energy spectral density has a smaller variance than a corresponding monochromatic component, so its scintillation index, defined as the ratio of variance to squared-mean-intensity, will be smaller than the unity value of the monochromatic component at saturation. When $\mu_F = 1$, or when $B \ll B_c$, Eq. (7) reduces to the exponential distribution described in Eq. (3).

The log-transformed bandwidth-averaged energy spectral density is defined as $L_{\mathcal{J}} = 10\log_{10}[\mathcal{J}/\mathcal{J}_{\text{ref}}]$, where the choice of reference level $\mathcal{J}_{\text{ref}}$ only adds a bias term to L_J. The probability distribution of $L_J = 10\log_{10}J$ is then described by

$$p(L_{\mathcal{J}}) = p(\mathcal{J} = 10^{L_{\mathcal{J}}/10})\left|\frac{d\mathcal{J}}{dL_{\mathcal{J}}}\right| = \frac{1}{(10\log_{10}e)\Gamma(\mu_F)}\left(\frac{\mu_F}{\bar{\mathcal{E}}}\right)^{\mu_F} 10^{\mu_F L_{\mathcal{J}}/10} \times \exp\left(-\mu_F\frac{10^{L_{\mathcal{J}}/10}}{\bar{\mathcal{E}}}\right), \text{ for } -\infty < L_{\mathcal{J}} < \infty, \tag{8}$$

which is an exponential-Gamma distribution.[2] The mean and standard deviation of $L_{\mathcal{J}}$ are derived in Appendix B and given by[2]

$$\langle L_{\mathcal{J}}\rangle = 10\log_{10}(\bar{\mathcal{E}}/\mu_F) + (10\log_{10}e)\frac{\Gamma'(\mu_F)}{\Gamma(\mu_F)}, \tag{9}$$

$$\sigma_{L_{\mathcal{J}}} = (10\log_{10}e)\sqrt{\zeta(2,\mu_F)} \approx 4.34\sqrt{\zeta(2,\mu_F)}, \tag{10}$$

respectively, where $\zeta(\nu,\ \mu_F)$ is the generalized Riemann zeta function

$$\zeta(\nu,\ \mu_F) = \sum_{k=0}^{\infty} \frac{1}{(k+\mu_F)^{\nu}}, \tag{11}$$

which converges to $\pi^2/6$ when $\mu_F = 1$ and $\nu = 2$, so that the standard deviation $\sigma_{L_{\mathcal{J}}} = 5.6$ dB.[11] Equations (10) and (11) show that a standard deviation smaller than 5.6 dB is obtained when μ_F is larger than 1. For a given data set, the number of frequency correlation cells μ_F can be found from the empirically determined standard deviation by solving Eq. (10). As shown in Ref. 2, when the number of correlation cells is large, $\mu_F \gg 1$, the standard deviation of $L_{\mathcal{J}}$ in Eq. (10) can be simplified to $\sigma_{L_{\mathcal{J}}} \simeq 4.34\sqrt{1/\mu_F}$.

When the broadband signal energy $E(f_m|t_k,B)$ obtained by integrating the energy spectral density over the signal bandwidth is considered

$$E(f_m|t_k,\ B) = B\mathcal{J}(f_m|t_k,\ B) = \int_{t_k}^{t_k+T_D} |\Psi(t)|^2 dt, \tag{12}$$

its probability density functions in both linear and log-transformed ($L_E = 10\log_{10}E$) quantities can be readily obtained

$$p(E) = \begin{cases} \dfrac{1}{\Gamma(\mu_F)}\left(\dfrac{\mu_F}{B\bar{\mathcal{E}}}\right)^{\mu_F} E^{(\mu_F-1)}\exp\left(-\mu_F\dfrac{E}{B\bar{\mathcal{E}}}\right), & \text{for } E \geq 0 \\ 0, & \text{elsewhere,} \end{cases} \tag{13}$$

and

$$p(L_E) = \frac{1}{(10\log_{10}e)\Gamma(\mu_F)}\left(\frac{\mu_F}{B\bar{\mathcal{E}}}\right)^{\mu_F} 10^{\mu_F L_E/10} \times \exp\left(-\mu_F\frac{10^{L_E}/10}{B\bar{\mathcal{E}}}\right), \quad -\infty < L_E < \infty, \tag{14}$$

respectively. The mean and standard deviation of the broadband signal energy in linear and log-transformed domains are then given by

$$\langle E\rangle = B\bar{\mathcal{E}}, \tag{15}$$

$$\sigma_E = \langle E\rangle/\sqrt{\mu_F}, \tag{16}$$

$$\langle L_E\rangle = 10\log_{10}\left(\frac{\langle E\rangle}{\mu_F}\right) + (10\log_{10}e)\frac{\Gamma'(\mu_F)}{\Gamma(\mu_F)}, \tag{17}$$

and

$$\sigma_{L_E} = (10\log_{10}e)\sqrt{\zeta(2,\ \mu_F)}, \tag{18}$$

respectively. Note that the log-transformed broadband signal energy L_E has a standard deviation identical to the log-transformed bandwidth-averaged energy spectral density $L_{\mathcal{J}}$, while their means differ by $10\log_{10}B$.

It should be noted that even though the measurement time is smaller than the signal correlation time ($T < \tau_c$) so that $\mu_T = 1$, the total number of correlation cells μ of the broadband signal obtained as the product $\mu = \mu_T\mu_F$ can still be larger than 1 when the signal bandwidth is larger than its correlation bandwidth, since then $\mu_F > 1$. This result then generalizes the derivation of Ref. 2 by also considering the correlation across the frequency components of a broadband waveform not addressed in Ref. 2. Here the broadband signal has Gamma distributed energy [see Eq. (13)] which reduces to the exponential distribution only when the signal bandwidth is smaller than its correlation bandwidth so that $\mu_F = 1$ as well for measurement times that satisfy $T < \tau_c$.

B. Probability distribution of broadband signal energy with a measurement time larger than the energy spectral density correlation time

We now consider the case when the measurement time T is larger than the correlation time τ_c of a broadband signal's energy spectral density components. We assume that the time separation between the arrival of any two broadband pulses $|t_i - t_j|$ is larger than the correlation time τ_c and that the broadband signal is statistically stationary over the measurement time T. Under these conditions, the measurements of the energy spectral densities of the broadband signal $\mathcal{E}(f|t_k)$ over time t_k for $k = 1,2,3,\ldots$ are independent fluctuations, each having an exponential distribution with identical mean and standard deviation both equal to $\bar{\mathcal{E}}$.

The time-averaged energy spectral density $\mathcal{S}(f)$ is

$$\mathcal{S}(f) = \frac{1}{N}\sum_{k=1}^{N}\mathcal{E}(f|t_k), \tag{19}$$

where N is the number of temporally independent broadband signals received over measurement time T. In this case, the number of temporal correlation cells is $\mu_T = N$. The probability density function for the time-averaged energy spectral density $\mathcal{S}(f)$ then has a characteristic function that can be obtained from the product of μ_T identical characteristic functions of the exponential distribution. This again leads to a Gamma distribution for $\mathcal{S}(f)$ given by

$$p(\mathcal{S}) = \begin{cases} \dfrac{1}{\Gamma(\mu_T)}\left(\dfrac{\mu_T}{\bar{\mathcal{E}}}\right)^{\mu_T}\mathcal{S}^{(\mu_T-1)}\exp\left(-\mu_T\dfrac{\mathcal{S}}{\bar{\mathcal{E}}}\right), & \text{for} \quad \mathcal{S} \geq 0 \\ 0, & \text{elsewhere.} \end{cases} \tag{20}$$

The time-averaged energy spectral density has mean $\bar{\mathcal{E}}$ and variance $\bar{\mathcal{E}}^2/\mu_T$. This time-averaged energy spectral density is equivalent to the time-averaged intensity W in Ref. 2, which has a probability distribution given by Eq. (9) of Ref. 2 and the number of correlation cells specified in that equation is μ_T. The distribution of the log-transformed time-averaged energy spectral density $L_S = 10\log_{10}\mathcal{S}(f)$ is

$$p(L_S) = \frac{1}{(10\log_{10}e)\Gamma(\mu_T)}\left(\frac{\mu_T}{\bar{\mathcal{E}}}\right)^{\mu_T} 10^{\mu_T L_S/10} \times \exp\left(-\mu_T\frac{10^{L_S/10}}{\bar{\mathcal{E}}}\right), \quad \text{for} -\infty < L_S < \infty, \tag{21}$$

which is an exponential-Gamma distribution[2] with mean and standard deviation given by

$$\langle L_{\mathcal{S}}\rangle = 10\log_{10}(\bar{\mathcal{E}}/\mu_T) + (10\log_{10}e)\frac{\Gamma'(\mu_T)}{\Gamma(\mu_T)}, \tag{22}$$

$$\sigma_{L_{\mathcal{S}}} = (10\log_{10}e)\sqrt{\zeta(2,\,\mu_T)}. \tag{23}$$

The time-averaged broadband signal energy with center frequency f_m and bandwidth B, averaged over measurement time T, is

$$E_T(f_m|B) = \frac{1}{N}\sum_{k=1}^{N} E(f_m|t_k,\,B), \tag{24}$$

where we assume as before that there are exactly $\mu_T = N$ statistically independent broadband signal receptions over the measurement time interval. The probability distribution for the time-averaged broadband signal energy is

$$p(E_T) = \begin{cases} \dfrac{1}{\Gamma(\mu)}\left(\dfrac{\mu}{\bar{\mathcal{E}}B}\right)^{\mu} {E_T}^{(\mu-1)}\exp\left(-\mu\dfrac{E_T}{B\bar{\mathcal{E}}}\right), & E_T \geq 0 \\ 0, & \text{elsewhere,} \end{cases} \tag{25}$$

where $\mu = \mu_F\mu_T$ is the total number of independent statistical fluctuations or correlation cells of the broadband signal averaged over the measurement time period and is expressed as the product of the number of correlation cells in frequency μ_F and the number of correlation cells in time μ_T. The mean and standard deviation of the time-averaged broadband signal energy are

$$\langle E_T\rangle = B\bar{\mathcal{E}}, \tag{26}$$

$$\sigma_{E_T} = \langle E_T\rangle/\sqrt{\mu_F\mu_T}. \tag{27}$$

The log transformed time-averaged broadband signal energy $L_{E_T} = 10\log_{10}E_T$ then has probability distribution, mean, and standard deviation given by

$$p(L_{E_T}) = \frac{1}{(10\log_{10}e)\Gamma(\mu)}\left(\frac{\mu}{B\bar{\mathcal{E}}}\right)^{\mu} 10^{\mu L_{E_T}/10} \times \exp\left(-\mu\frac{10^{L_{E_T}/10}}{B\bar{\mathcal{E}}}\right), \quad -\infty < L_{E_T} < \infty, \tag{28}$$

where $\mu = \mu_F\mu_T$ and

$$\langle L_{E_T}\rangle = 10\log_{10}\left(\frac{\langle E_T\rangle}{\mu_F\mu_T}\right) + (10\log_{10}e)\frac{\Gamma'(\mu_F\mu_T)}{\Gamma(\mu_F\mu_T)}, \tag{29}$$

$$\sigma_{L_{E_T}} = (10\log_{10}e)\sqrt{\zeta(2,\,\mu_F\mu_T)}, \tag{30}$$

respectively.

Finally, in analogy to the correlation bandwidth defined in Eq. (6), we define the correlation time of the broadband signal's energy spectral density component as

$$\tau_c(f_m) = \int_{-\infty}^{\infty} \rho(\xi = 0,\,\tau|f_m)d\tau. \tag{31}$$

III. BROADBAND TRANSMISSION SCINTILLATION STATISTICS FROM THE 2006 GULF OF MAINE EXPERIMENT

A. Experimental data collection and processing

The GOME'06 (Refs. 5 and 6) conducted from September 19 to October 6, 2006 near the northern flank of Georges Bank [Fig. 1(A)] was sponsored by the Sloan Foundation and the Office of Naval Research. A vertical source array was used to transmit broadband Tukey-windowed linear frequency modulated pulses each of 1 s duration and 50 Hz bandwidth with azimuthal symmetry at four distinct center frequencies: 415, 735, 950, and 1125 Hz. The pulse repetition interval was 150 s at each center frequency. The signals were received on a towed horizontal line array[5,6,31] of which one hydrophone was desensitized with a lower gain setting, giving it a larger dynamic range for recording the one-way propagated waveforms. The tow tracks of the receiver array are shown in Fig. 1(A) with a mean tow speed of 2 m/s. The source-receiver separations varied between 1 and 20 km, with over 80% of the transmissions occurring in the 4 to 12 km range [Fig. 1(B)]. The source array was centered at a depth of between 60 and 70 m while the receiver array was centered at 105 m depth with typical depth variation of up to 10 m. The water depth at the location where the data was acquired was fairly level with an average of roughly 200 m.

The water-column temperature and salinity were measured using expendable bathythermographs (XBTs) and conductivity-temperature-depth (CTD) sensors. The derived

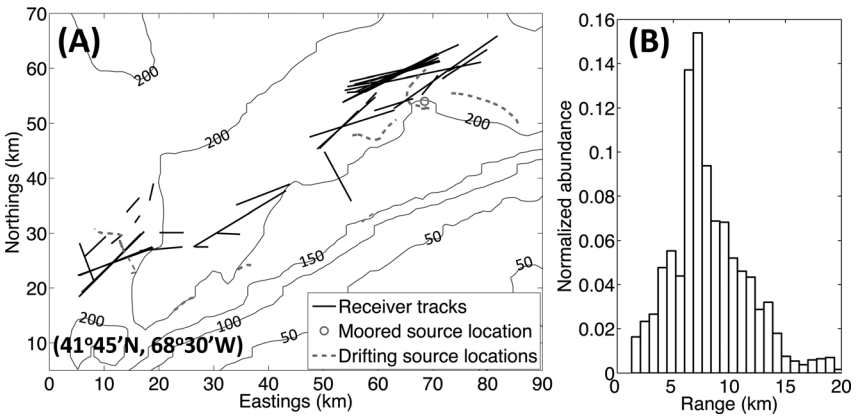

FIG. 1. (A) Locations of source and receiver during GOME'06 (Refs. 5 and 6). Isobath contours have the unit of *m*. The sound speed profiles shown in Fig. 2(A) were collected roughly at the beginning, middle, and end of each receiver track and at the source locations. (B) Normalized histogram of the number of transmissions as a function of source and receiver separation or range.

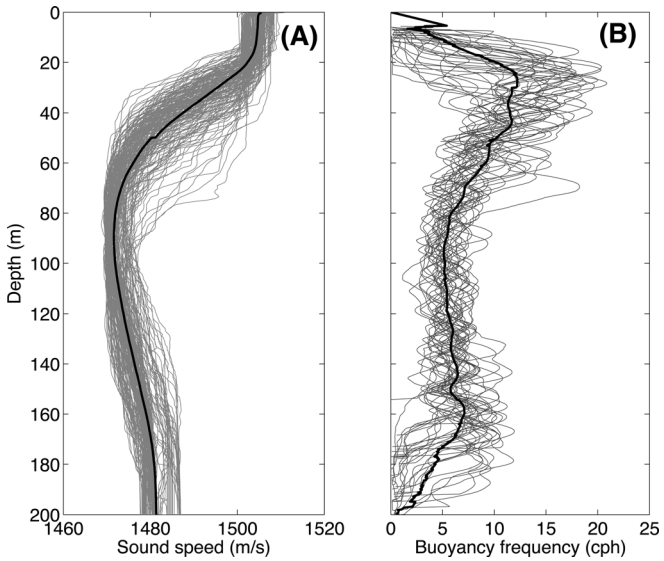

FIG. 2. (A) Sound speed profiles and (B) buoyancy frequency profiles obtained from XBT and CTD measurements at the experimental site. A total of 185 sound speed profiles and 35 buoyancy frequency profiles are shown.

water-column sound speed and buoyancy frequency profiles are shown in Fig. 2 and contain 185 samples for the sound speed profiles and 35 samples for the buoyancy frequency profiles. Other details about the measurement geometry and oceanographic properties of the environment are provided in Sec. II of Ref. 6.

An example of the source waveform and the propagated signal received on the desensitized hydrophone at a source-receiver separation of 7.6 km are shown in Fig. 3. Fluctuations of the received signal can be observed over both its time duration and bandwidth.

The received broadband signals were processed following the approach outlined in Sec. II B of Ref. 16 to determine the signal energies. Let $\psi(\boldsymbol{r}|\boldsymbol{r}_0,t)$ be the received pressure in time t at receiver location $\boldsymbol{r}$ from a source located at $\boldsymbol{r}_0$. The complex spectral amplitude $\Phi(\boldsymbol{r}|\boldsymbol{r}_0,f)$ is obtained by Fourier transform analysis

$$\Phi(\boldsymbol{r}|\boldsymbol{r}_0,f) = \int_T \Psi(\boldsymbol{r}|\boldsymbol{r}_0,t)e^{j2\pi ft}dt, \tag{32}$$

where T is the time window used to isolate the direct arrival from reverberation and other noise sources. The time window was 2 s long, including 0.5 s before the initial arrival and 0.5 s after the 1 s signal duration to sufficiently capture the signal and its later arrivals.[16] The energy spectral density is next calculated via

$$\mathcal{E}(\boldsymbol{r}|\boldsymbol{r}_0,f) = |\Phi(\boldsymbol{r}|\boldsymbol{r}_0,f)|^2. \tag{33}$$

The bandwidth-averaged energy spectral density $\mathcal{J}(\boldsymbol{r}|\boldsymbol{r}_0,f_m,B)$ is then calculated as a function of bandwidth B and center frequency f_m for each received waveform

$$\mathcal{J}(\boldsymbol{r}|\boldsymbol{r}_0,f_m,B) = \frac{1}{B}\int_{f_m-B/2}^{f_m+B/2} \mathcal{E}(\boldsymbol{r}|\boldsymbol{r}_0,f)df. \tag{34}$$

The log-transformed bandwidth-averaged energy spectral density level $L_{\mathcal{J}} = 10\log_{10}[\mathcal{J}(\boldsymbol{r}|\boldsymbol{r}_0,f_m,B)/\mathcal{J}_{\text{ref}}]$ was then calculated for each center frequency f_m and bandwidth B. The broadband signal energy $E(\boldsymbol{r}|\boldsymbol{r}_0,f_m,B)$ is calculated using

$$E(\boldsymbol{r}|\boldsymbol{r}_0,f_m,B) = B\mathcal{J}(\boldsymbol{r}|\boldsymbol{r}_0,f_m,B) = \int_{f_m-B/2}^{f_m+B/2} \mathcal{E}(\boldsymbol{r}|\boldsymbol{r}_0,f)df, \tag{35}$$

and its log-transform is $L_E = 10\log_{10}[E(\boldsymbol{r}|\boldsymbol{r}_0,f_m,B)/E_{\text{ref}}]$.

Standard deviations $\sigma_{L_{\mathcal{J}}}$ were first calculated for transmissions within a running range window of 2 km length in each track and then averaged across tracks. The 50 Hz bandwidth Tukey-windowed signals had 5 Hz tapered on either side of the spectrum so that their effective bandwidth was

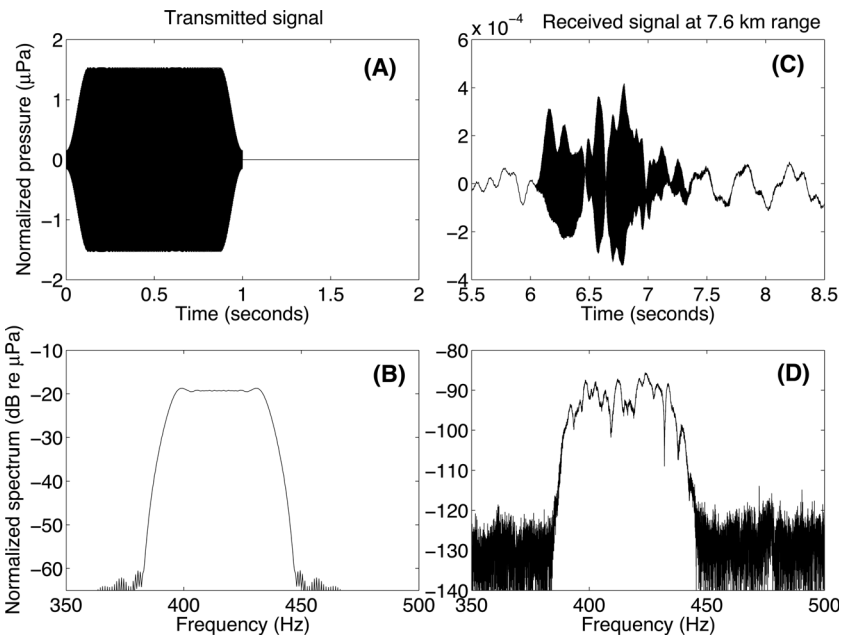

FIG. 3. Example of source waveform and received broadband signal at a range of 7.6 km for the Tukey-windowed linear frequency modulated pulse centered at $f_m = 415$ Hz. (A) Source waveform, (B) source spectrum, (C) received signal waveform, and (D) received signal spectrum. The results are normalized for a 0 dB re 1 μPa at 1 m source level.

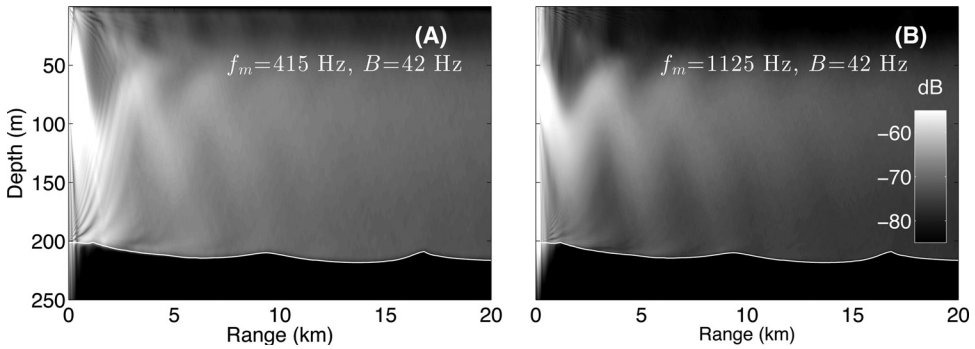

FIG. 4. Modeled transmission loss for 50-Hz bandwidth Tukey-windowed broadband signals centered at (A) $f_m = 415$ Hz and (B) $f_m = 1125$ Hz, calculated using the range-dependent parabolic equation model (Ref. 34). Transmission losses are obtained by averaging over 20 independent Monte Carlo realizations of the broadband signal in the Gulf of Maine environment randomized by internal waves.

only 42 Hz. It should be noted that the 1 s time duration of the transmitted signals is much shorter than their energy spectral density correlation time scale of fluctuation which is expected to be on the order of several minutes.[32,33]

We model the broadband transmission losses for the 50 Hz bandwidth Tukey-windowed linear frequency modulated signals centered at $f_m = 415$ Hz and $f_m = 1125$ Hz transmitted from a vertical source array for one example of the source-receiver geometry identical to the experiment in Fig. 4. The transmission losses are calculated using a range-dependent parabolic equation model.[34] The bottom is assumed to be sandy with a sound speed of $c_b = 1700$ m/s, density $\rho_b = 1.9$ g/cm^2, and attenuation coefficient of 0.8 dB/λ.[6] The results are plotted after averaging over 20 independent Monte Carlo realizations of the broadband signal energy in a waveguide randomized by internal waves.[6,16] The acoustic field has negligible surface interaction but significant bottom interaction due to the downward refracting sound speed profile for the source depth of 65 m. This significant bottom interaction will cause the acoustic field to become fully randomized and saturated at source-receiver ranges roughly ten times the water depth.

B. Probability distribution of log-transformed bandwidth-averaged energy spectral densities

Histograms of the log-transformed bandwidth-averaged energy spectral densities $L_{\mathcal{J}}(\boldsymbol{r}|\boldsymbol{r}_0, f_m, B)$ for the approximately monochromatic components with $B = 0.5$ Hz bandwidth and for the $B = 42$ Hz effective bandwidth Tukey windowed signals centered at $f_m = 415$ Hz and $f_m = 1125$ Hz are plotted in Fig. 5 for transmission data having source-receiver separations between 7 and 9 km. The histogram is created from roughly 400 broadband signal receptions at each center frequency. The measured number of frequency correlation cells μ_F indicated in Fig. 5 is obtained using Eq. (10) after standard deviations $\sigma_{L_{\mathcal{J}}}$ were calculated in each case. The theoretical exponential-Gamma distribution described by Eq. (8) with measured mean intensity $\bar{\mathcal{E}}$ and number of frequency correlation cells μ_F as parameters are plotted for each case in Fig. 5. The exponential-Gamma distribution of Eq. (8) with assumed $\mu_F = 1$ is also shown for comparison. It should be noted that these distributions would correspond to the exponential distribution when $\mu_F = 1$ and the Gamma distribution when $\mu_F > 1$ if the linear quantities were plotted instead.

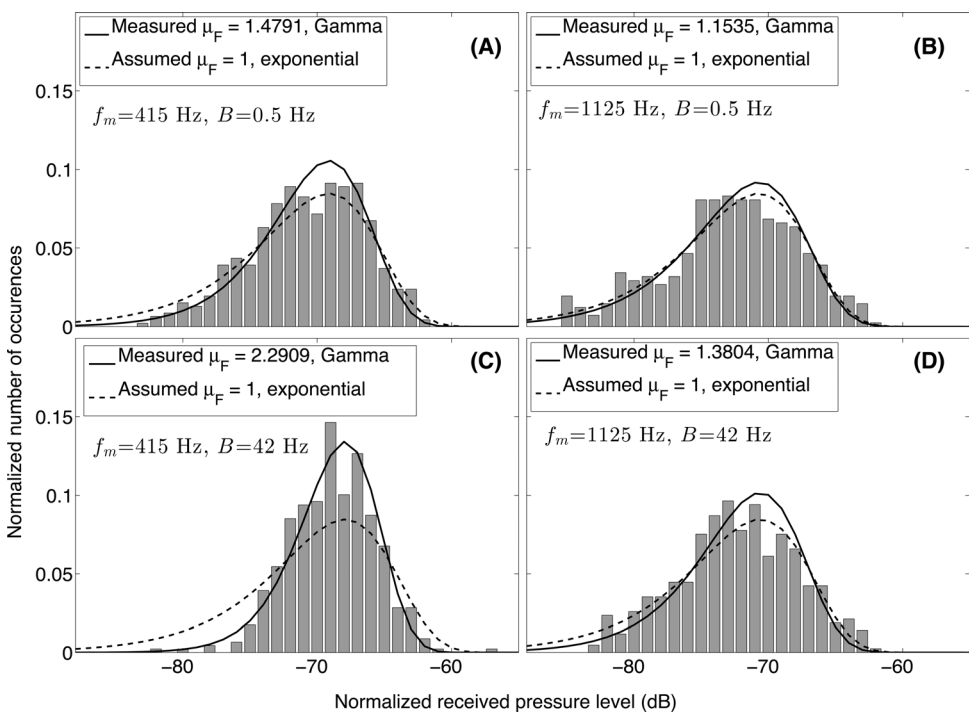

FIG. 5. Histograms showing distribution of measured log-transformed bandwidth-averaged energy spectral densities $L_{\mathcal{J}}$ received in the 7 to 9 km range for two center frequencies $f_m = 415$ Hz (left) and $f_m = 1125$ Hz (right) with (A) and (B) 0.5 Hz bandwidth (nearly monochromatic components), and (C) and (D) 50 Hz bandwidth Tukey windowed signals with an effective bandwidth of 42 Hz. The histograms are overlain with the theoretical exponential-Gamma distribution modeled using Eq. (8) (black curve), with the number of frequency correlation cells μ_F determined from the data mean and standard deviation. The exponential-Gamma distribution corresponding to assumed $\mu_F = 1$ is also shown for comparison.

TABLE I. Two-sided chi-squared test results to verify the distributions of the log-transformed bandwidth-averaged energy spectral density $L_{\mathcal{J}}$ for the four scenarios shown in Fig. 5. A significance level of $\alpha = 0.05$ gives χ^2 within the range from lower-tail to upper-tail critical values for both the Gamma and exponential distributions.

f_m (Hz)	B (Hz)	Number of bins (N)	μ_F	χ^2 (Gamma)	χ^2 (Exponential)	$\chi^2_{\text{critical, lower}}$ ($\alpha = 0.05$)	$\chi^2_{\text{critical, upper}}$ ($\alpha = 0.05$)
415	0.5	19	1.48	27.78	15.28	8.91	30.14
415	42	13	2.29	20.61	55.55	5.00	22.24
1125	0.5	20	1.15	19.15	18.10	9.59	28.87
1125	42	18	1.38	29.84	20.40	8.23	31.53

For the signals with center frequency $f_m = 415$ Hz, the number of frequency correlation cells μ_F increased from 1.48 to 2.29 as the bandwidth increased from 0.5 to 42 Hz, since there was a corresponding reduction in the standard deviation, as will be shown in Sec. III C. For the higher frequency signals centered at $f_m = 1125$ Hz, the number of frequency correlation cells μ_F increased only slightly from 1.15 to 1.38 when the bandwidth increased.

We perform a two-sided chi-squared test[13] with a significance level $\alpha = 0.05$ to quantify the goodness of fit of the bandwidth-averaged energy spectral density levels $L_{\mathcal{J}}$ with the exponential-Gamma distributions parameterized by either assumed $\mu_F = 1$ (corresponding to exponential distribution for linear quantity) or the value of $\mu_F > 1$ experimentally obtained from the measured standard deviations (corresponding to Gamma distribution for the linear quantity). The results are tabulated in Table I. For the approximately monochromatic components ($B = 0.5$ Hz) with experimentally determined μ_F close to 1, the χ^2 values are within the critical bounds of the corresponding degree of freedom so that both the exponential and Gamma distributions are considered acceptable for the linear quantity. It should be noted that this is expected since the Gamma distribution converges to the exponential distribution when $\mu_F = 1$. For the 42 Hz effective bandwidth signals centered at $f_m = 415$ Hz with experimentally determined $\mu_F = 2.29$, the exponential distribution for the linear quantity is rejected because χ^2 is much larger than the upper critical value. For this case, the Gamma distribution is accepted by the chi-squared test and provides a better match to the data for the linear quantity. For the 42 Hz effective bandwidth signals centered at $f_m = 1125$ Hz, both distributions are acceptable based on the chi-squared test since the experimentally determined μ_F is still close to 1.

C. Mean and standard deviation of energy spectral density across signal bandwidth

A basic assumption of the statistical theory presented in Sec. II is that the frequency components of a broadband signal are each saturated, so that the energy spectral density components $\mathcal{E}(\boldsymbol{r}|\boldsymbol{r}_0,f)$ follow the exponential distribution with 5.6 dB standard deviation and a mean that is approximately constant across the signal bandwidth. In Sec. III B, we showed the energy spectral density of the center frequency component of the received broadband signals in the Gulf of Maine is well matched to the exponential distribution. A similar result is obtained when we consider the energy spectral density distribution of other frequency components of the signals.

In Fig. 6, we plot the mean and standard deviation of the log-transformed energy spectral densities $L_{\mathcal{E}} = 10\log_{10}[\mathcal{E}(\boldsymbol{r}|\boldsymbol{r}_0,f)/\mathcal{E}_{\text{ref}}]$ of the received broadband signals in the 7 to 9 km range centered at $f_m = 415$ and 1125 Hz, as a function of frequency after source level correction. Roughly 400 received broadband signals were used in the calculation. The mean level stays relatively constant across the signal bandwidth for both waveforms, and standard deviations are close to the saturation value of 5.6 dB for all frequencies across the signal bandwidth. This validates our assumption of saturated frequency components with equal means for the received broadband signals.

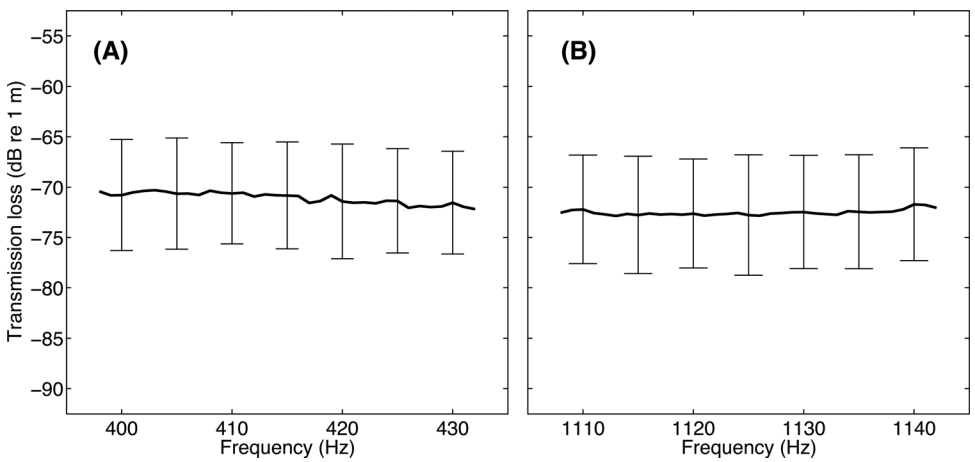

FIG. 6. Mean and standard deviation of the log-transformed energy spectral density $L_{\mathcal{E}}$ as a function of frequency for broadband signals received between the 7 and 9 km range, centered at (A) $f_m = 415$ Hz and (B) $f_m = 1125$ Hz.

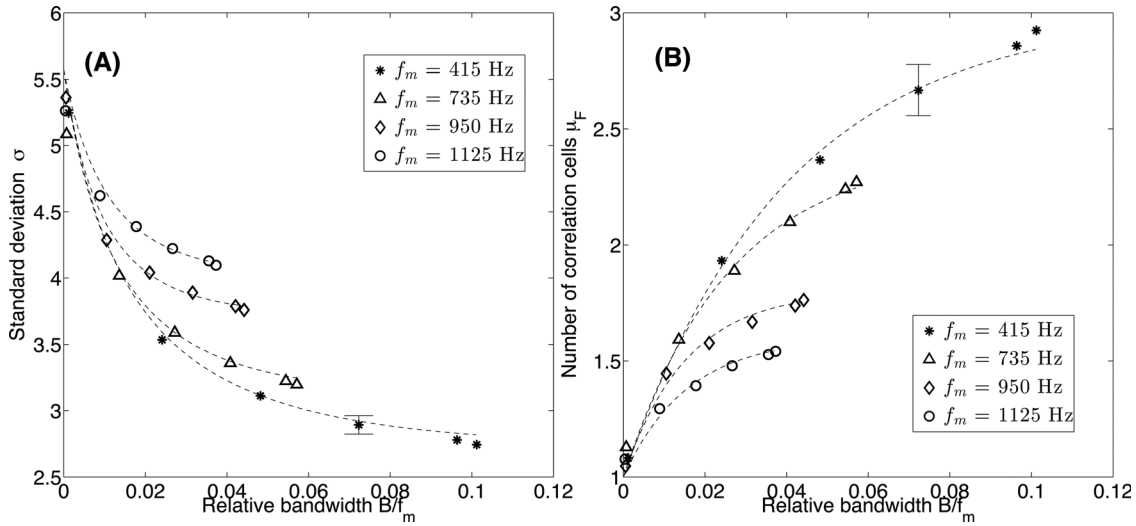

FIG. 7. (A) Empirically measured standard deviations of the log-transformed bandwidth-averaged energy spectral densities $L_{\mathcal{J}}$ obtained from broadband transmissions in the Gulf of Maine shown as points. (B) The number of frequency correlation cells μ_F are obtained from the measured signal standard deviations via Eq. (10). The dotted curves in (A) and (B) are obtained from the minimum mean-squared error fit to the data points using the equation and coefficients in Table II. The error bar shown applies to all data points.

D. Dependence of signal energy standard deviation and scintillation index on bandwidth and center frequency

The measured standard deviations of the log-transformed bandwidth-averaged energy spectral densities $L_{\mathcal{J}}$ averaged over all tracks and source-receiver ranges are plotted as functions of center frequency f_m and relative bandwidth B/f_m in Fig. 7. The standard deviations approach 5.6 dB only for the approximately monochromatic components but decrease gradually with increasing bandwidth for the broadband signals. For signals with equivalent relative bandwidths, $B/f_m =$ constant, the signal with the lower center frequency has a smaller standard deviation. The error in the mean standard deviation estimates shown in the plot is small, approximately 0.02 dB, and the same for all 4 center frequencies and bandwidths shown since roughly 1800 distinct broadband transmissions at each center frequency were used in the analysis.

The number of frequency correlation cells μ_F calculated from the standard deviations by solving Eq. (10) are plotted as a function of center frequency and relative bandwidth in Fig. 7(B). When the signal bandwidth approaches zero or when the signal becomes monochromatic, μ_F converges to one at all four center frequencies, which corresponds to the case of unity time-bandwidth signals described in Refs. 2 and 11. For the broadband signals with larger bandwidths, the number of frequency correlation cells μ_F is larger than 1. Curve fitting with an inverted exponential decay function shows that the number of frequency correlation cells is higher for signals with lower center frequencies. This relationship is tabulated in Table II. While the experimental data have a maximum effective bandwidth of 42 Hz, it is expected that μ_F will continue to increase with bandwidth, further reducing the standard deviation. Note that since the log-transformed broadband signal energies L_E have identical standard deviations to the log-transformed bandwidth-averaged energy spectral densities $L_{\mathcal{J}}$ [compare Eqs. (10) and (18)], the results obtained here regarding the measured standard deviations and their dependencies also apply to the signal energies L_E.

The SIs for the bandwidth-averaged energy spectral densities $\mathcal{J}(\boldsymbol{r}|\boldsymbol{r}_0,f)$ at the four center frequencies f_m are plotted as a function of relative bandwidth B/f_m in Fig. 8. Consistent with the theory developed in Sec. II, the SIs are smaller than 1 for all broadband signals, and decrease with increasing bandwidth. The SIs approach 1 only when the signal bandwidths are small enough to be nearly monochromatic. For the signals with identical relative bandwidths, $B/f_m =$ constant, a smaller scintillation index is obtained at the lower center frequency f_m. Since the broadband signal energies E can be obtained from the bandwidth-averaged energy spectral densities J by multiplication with the signal bandwidth [see Eqs. (12) and (35)], they have identical measured SIs and the results obtained here also apply to the broadband signal energies.

The results in Fig. 8 are consistent with the assumption made in the theory of Sec. II that the energy spectral density components of the broadband signal have unity SIs because they are saturated. It should be noted that the results presented here do not provide any information on the approach

TABLE II. Empirically determined number of frequency correlation cells μ_F is related to relative bandwidth B/f_m by the "inverted exponential decay" relationship $\mu_F = A - (A-1)\exp(-kB/f_m)$, with coefficients A and k determined by curve fitting as shown in Fig. 7. The case $(B=0,\ \mu_F=1)$ corresponds to one unique independent fluctuation. When B becomes very large, μ_F tends to A, its upper saturation value for each center frequency, which is 3 for the lowest frequency $f_m = 415$ Hz and 1.6 for the highest frequency $f_m = 1125$ Hz.

f_m (Hz)	A	k
415	3	25.2
735	2.4	38.5
950	1.8	65.1
1125	1.6	63.6

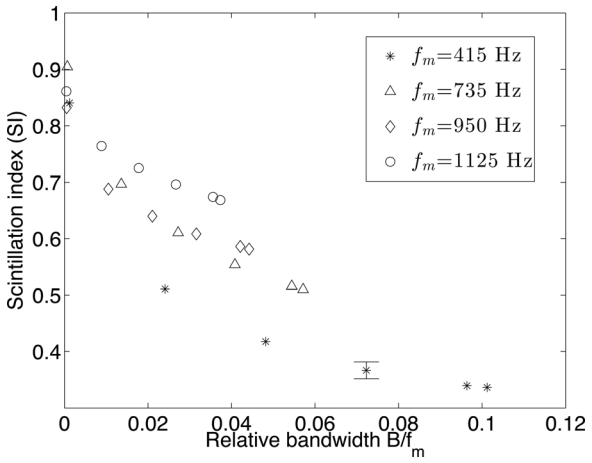

FIG. 8. Measured SIs in the Gulf of Maine for all four center frequencies as a function of relative bandwidth. The error bar shown applies to all data points.

to saturation discussed in Refs. 15 and 35. This is because the present data set were acquired at a largely 4 to 12 km ranges where the signals were already fully saturated. To determine the approach to saturation, measurements at much shorter ranges <3 km would be needed,[16] where they are expected to transition from the unsaturated to the partially saturated[12] and then fully saturated regimes.

E. Energy spectral density correlation bandwidth from measured broadband data

The energy spectral density frequency correlation coefficients $\rho(\xi,\ \tau = 0|f_m)$ are calculated for the broadband signals at each of the four center frequencies using Eq. (A11) and plotted in Fig. 9. Broadband received signals with higher center frequencies have larger energy spectral density correlation bandwidths since their correlation coefficients decay much slower with a frequency shift ξ from the center frequency f_m. From Fig. 9, the correlation coefficient for the broadband signal with center frequency $f_m = 415$ Hz has an e-folding bandwidth of approximately 35 Hz, implying that there are two frequency correlation cells within its 50 Hz physical bandwidth. This result is consistent with the

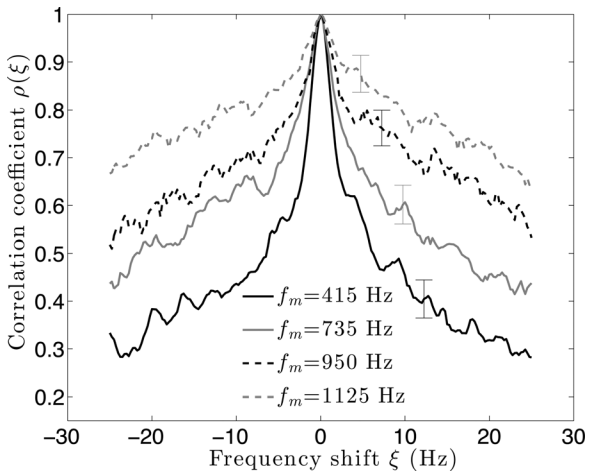

FIG. 9. Average energy spectral density correlation coefficient $\rho(\xi,\ \tau = 0|f_m)$ calculated from received broadband signals at the four center frequencies shown as a function of frequency shift within the signal bandwidth.

inferred value of μ_F from the measured standard deviation shown in Fig. 7(B) for center frequency $f_m = 415$ Hz. The broadband signal with center frequency $f_m = 1125$ Hz, on the other hand, is highly correlated across its physical bandwidth, having correlation coefficient values $\rho(\xi,\ \tau = 0|1125) > 0.6$. This implies that the number of frequency correlation cells μ_F is close to 1 for the received signals with a center frequency $f_m = 1125$ Hz, consistent with the results obtained by considering the standard deviations in Fig. 7. An exponential decay fit for $\rho(\xi,\ \tau = 0|f_m)$ gives the energy spectral density relative correlation bandwidth B_c/f_m of roughly $8.5\% \pm 2\%$ for all four center frequencies.

When the signal bandwidth B is sufficiently large, the number of frequency correlation cells μ_F can also be approximated[2] from the linear relationship, $\mu_F \approx B/B_c$. This is equivalent to $\mathrm{d}\mu_F/\mathrm{d}(B/f_m) \approx f_m/B_c$, which enables an estimate of the correlation bandwidth B_c to be obtained from the gradient of the plot of μ_F versus relative bandwidth B/f_m in Fig. 7. By applying a linear curve fit to the last four data points for each center frequency f_m where the trend of μ_F is relatively linear, we obtain relative correlation bandwidths B_c/f_m of $9.5\% \pm 2\%$ at the four center frequencies. This is a rough estimate, however, since B is not significantly larger than B_c for all four broadband waveforms. Signals with much larger physical bandwidths are required in order to more accurately quantify the correlation bandwidth as a function of center frequency.

The approximately 10% energy spectral density correlation bandwidth of the received ocean-acoustic broadband signals correspond to roughly a whole tone in the chromatic scale of music. This implies that given a short-duration broadband signal with arbitrary bandwidth B, the number of energy spectral density frequency correlation cells after forward propagation through the random ocean waveguide can be easily approximated by subdividing the physical bandwidth into the number of whole tones.

F. Temporal averaging and broadband spectrum reconstruction in a random multi-modal range-dependent ocean waveguide

When averaging the received broadband signal energy spectral densities over a measurement time larger than the correlation time, the theory in Sec. II B suggests that the total number of correlation cells $\mu = \mu_T \mu_F$ will be increased, leading to smaller standard deviations across all the frequency components. Figure 10 shows the log-transformed time-averaged energy spectral density L_S plotted as a function of frequency estimated from all broadband transmissions within the 7 to 9 km range for waveforms with center frequencies $f_m = 415$ Hz and $f_m = 1125$ Hz. The error in the time-averaged energy spectral density estimates are significantly reduced from 5.6 dB for a single sample to less than 0.6 dB. The time-averaged energy spectral density of the received broadband signals in Fig. 10 provides an excellent reconstruction of the original Tukey-windowed spectrum [compare Fig. 10(A) with Fig. 3(B)]. In contrast, the spectrum obtained from an individual received signal [see Fig. 3(D)]

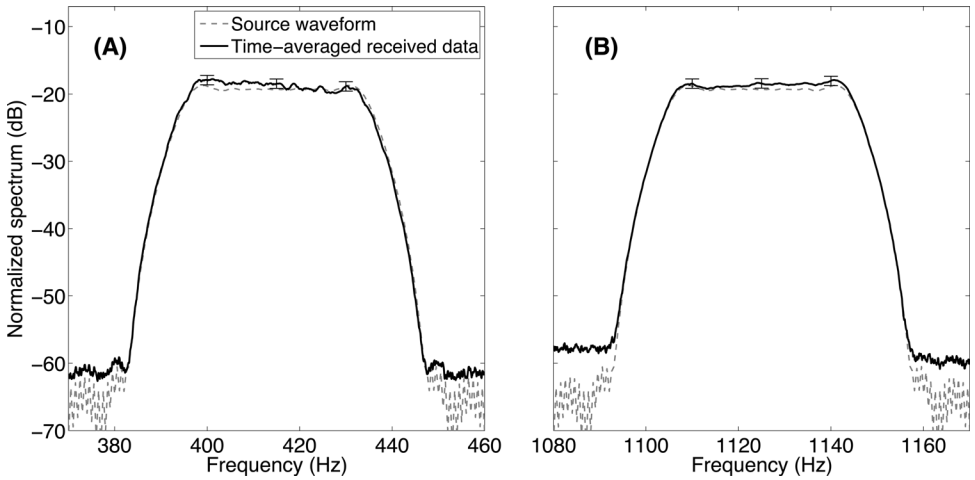

FIG. 10. Log-transformed time-averaged energy spectral density L_S calculated from received broadband signals in the 7 to 9 km range for the waveforms centered at (A) $f_m = 415$ Hz and (B) $f_m = 1125$ Hz.

is highly distorted with as large as 6 dB variation across the signal bandwidth from multi-modal interference.

G. Discussion and comparison to other shallow water measurements

Previous measurements[15,16] of broadband signal energy standard deviations in other shallow water waveguides are consistent with the statistical theory and experimental results presented here. For instance, in the continental shelf environment off Long Island, New York, broadband acoustic signals with bandwidths up to 150 Hz at various center frequencies from 300 to 1500 Hz propagated between the 2 and 10 km range from a source array in 80 m water depth were measured with standard deviations between 2.9 and 4 dB[16] for the signal energies. The broadband signal energies were also found to follow the Gamma distribution. In Ref. 16, it was shown through the center frequency component of the broadband signal that the energy spectral density of the Fourier components were statistically saturated with roughly 5.6 dB standard deviation and a distribution that matched the exponential. In Ref. 15, broadband signals with 100 Hz bandwidth centered at 400 Hz propagated through the New England continental shelf environment approximately 200 m deep were measured with standard deviations of approximately 2 dB at 40 to 50 km range. This is smaller than the characteristic 5.6 dB standard deviation of a monochromatic signal. Furthermore, it was shown in Ref. 15 that the distribution of the point intensity closely followed an exponential distribution, approximating an instantaneous measurement of a statistically saturated acoustic field. The broadband signals in Refs. 15 and 16 both had durations smaller than their correlation time.

IV. CONCLUSION

The probability distribution for saturated broadband ocean-acoustic signal energy has been derived using coherence theory as a function of the signal bandwidth, measurement time, frequency correlation, and temporal correlation of its energy spectral density. The derivation assumes the broadband signal is composed of frequency components from Fourier analysis that are *each* fully saturated with energy spectral density that obey the exponential distribution with 5.6 dB standard deviation and unity scintillation index. When the signal bandwidth and measurement time are larger than the correlation bandwidth and correlation time of its energy spectral density components, respectively, the broadband signal energy obtained by integrating the energy spectral density across the signal bandwidth then follows the Gamma distribution. The broadband signal energy has a standard deviation that can be significantly smaller than 5.6 dB and a scintillation index less than unity. This is because forward propagation and scattering through the random ocean environment causes the broadband signal to decorrelate across its bandwidth or over time. The theory is verified with broadband transmissions in the Gulf of Maine shallow water waveguide in the 300 to 1200 Hz frequency range. The transmissions were found to be saturated, where the exponential distribution and standard deviation near 5.6 dB were observed for the energy spectral density components of the measured signals. The bandwidth-integrated signal energies matched well with the Gamma distribution with standard deviations ranging from 2.7 to 4.6 dB for effective bandwidths up to 42 Hz. The measured standard deviations and SIs were found to be smaller for signals with lower center frequencies and larger bandwidths. The energy spectral density correlation bandwidths of the broadband signals were found to be larger for signals with higher center frequencies, and can be approximated as roughly 10% of the center frequency.

ACKNOWLEDGMENT

This research was funded by the Office of Naval Research Ocean Acoustics Program.

APPENDIX A: MEAN AND STANDARD DEVIATION OF BANDWIDTH AVERAGED ENERGY SPECTRAL DENSITY

Here we derive expressions for the mean $\bar{\mathcal{J}}$ and standard deviation $\sigma_{\mathcal{J}}$ of the bandwidth averaged energy spectral density. The mean value of $\mathcal{J}(f_m|t_k,\ B)$ can be obtained by starting with Eq. (4) and interchanging the order of integration and expectation

$$\langle \mathcal{J}(f_m|t_k,B)\rangle = \left\langle \frac{1}{B}\int_{f_m-B/2}^{f_m+B/2} \mathcal{E}(f|t_k)df \right\rangle \tag{A1}$$

$$= \bar{\mathcal{E}}. \tag{A2}$$

The variance of $\mathcal{J}(f_m|t_k,\ B)$ is

$$\sigma^2_{\mathcal{J}}(f_m|B) = \langle(\mathcal{J}(f_m|t_k,B))^2\rangle - \langle\mathcal{J}(f_m|t_k,B)\rangle^2 \tag{A3}$$

$$= \left\langle \left[\frac{1}{B}\int_{f_m-B/2}^{f_m+B/2} \mathcal{E}(f|t_k)df\right]^2 \right\rangle - \bar{\mathcal{E}}^2 \tag{A4}$$

$$= \frac{1}{B^2}\int_{f_m-B/2}^{f_m+B/2}\int_{f_m-B/2}^{f_m+B/2} \langle\mathcal{E}(f|t_k)\mathcal{E}(f'|t_k)\rangle df\, df' - \bar{\mathcal{E}}^2 \tag{A5}$$

$$= \frac{1}{B^2}\int_{f_m-B/2}^{f_m+B/2}\int_{f_m-B/2}^{f_m+B/2} R_{\mathcal{E}}(f-f',\tau=0|f_m)df\, df' - \bar{\mathcal{E}}^2, \tag{A6}$$

where $R_{\mathcal{E}}(\xi,\ \tau|f_m)$ is the joint temporal-spectral autocorrelation function of the energy spectral density $\mathcal{E}(f|t_k)$ for a frequency shift $\xi = f - f'$ and time shift τ defined by

$$R_{\mathcal{E}}(\xi,\tau|f_m) = \langle\mathcal{E}(f|t)\mathcal{E}(f+\xi|t+\tau)\rangle \tag{A7}$$

$$= \langle\Phi(f|t)\Phi^*(f|t)\Phi(f+\xi|t+\tau)\Phi^*(f+\xi|t+\tau)\rangle, \tag{A8}$$

or equivalently the fourth-order joint temporal-spectral coherence function of the complex spectral amplitude $\phi(f|t)$ as defined in Eq. (A8). The integrand in Eq. (A6) can be approximated as an even function of $(f-f')$, so the double integral can be reduced to a single integral leading to

$$\sigma^2_{\mathcal{J}}(f_m|B) = \frac{1}{B}\int_{-\infty}^{\infty}\Delta\left(\frac{\xi}{B}\right)R_{\mathcal{E}}(\xi,\tau=0|f_m)d\xi - \bar{\mathcal{E}}^2, \tag{A9}$$

for the variance of $\mathcal{J}(f_m|B)$, where

$$\Delta\left(\frac{\xi}{B}\right) = \begin{cases} 1-\left|\frac{\xi}{B}\right| & \text{for}\left|\frac{\xi}{B}\right| \le 1, \\ 0, & \text{elsewhere}, \end{cases} \tag{A10}$$

is the triangular function arising from the autoconvolution of the rectangular window of width B.

We next express the joint temporal-spectral autocorrelation function $R_{\mathcal{E}}(\xi,\ \tau|f_m)$ in terms of the joint temporal-spectral correlation coefficient $\rho(\xi,\ \tau|f_m)$ of the energy spectral density defined as

$$\rho(\xi,\tau|f_m) = \frac{\langle[\mathcal{E}(f|t)-\bar{\mathcal{E}}(f|t)][\mathcal{E}(f+\xi|t+\tau)-\bar{\mathcal{E}}(f+\xi|t+\tau)\rangle}{\sigma^2_{\mathcal{E}}}. \tag{A11}$$

Assuming that $\mathcal{E}(f|t)$ and $\mathcal{E}(f+\xi|t+\tau)$ are both exponentially distributed with identical mean and standard deviations which are equal to $\bar{\mathcal{E}}$, $\rho(\xi,\ \tau|f_m)$ can then be written in the form

$$\rho(\xi,\ \tau|f_m) = \frac{\langle\mathcal{E}(f|t)\mathcal{E}(f+\xi|t+\tau)\rangle - \bar{\mathcal{E}}^2}{\bar{\mathcal{E}}^2}, \tag{A12}$$

so that

$$R_{\mathcal{E}}(\xi,\tau|f_m) = \bar{\mathcal{E}}^2[1+\rho(\xi,\tau|f_m)]. \tag{A13}$$

Substituting Eq. (A13) into Eq. (A9) yields the result

$$\sigma^2_{\mathcal{J}}(f_m|B) = \bar{\mathcal{E}}^2\left[\frac{1}{B}\int_{-\infty}^{\infty}\Delta\left(\frac{\xi}{B}\right)\rho(\xi,\tau=0|f_m)d\xi\right]. \tag{A14}$$

In Eq. (5), we identify $B[\int_{-\infty}^{\infty}\Delta(\xi/B)\rho(\xi,\tau=0|f_m)\ d\xi]^{-1} = \mu_F$ as the number of frequency correlation cells of the energy spectral density, so that the variance of the bandwidth averaged energy spectral density can be expressed as

$$\sigma^2_{\mathcal{J}}(f_m|B) = \bar{\mathcal{E}}^2/\mu_F. \tag{A15}$$

APPENDIX B: MEAN AND STANDARD DEVIATION OF LOG-TRANSFORMED BANDWIDTH-AVERAGED ENERGY SPECTRAL DENSITY

Here we derive expressions for the mean $\langle L_{\mathcal{J}}\rangle$ and standard deviation $\sigma_{L_{\mathcal{J}}}$ of the log-transformed bandwidth averaged energy spectral density. First note that a change of logarithmic base gives

$$L_{\mathcal{J}} = 10\log_{10}\mathcal{J} = 10\log_{10}e\ln\mathcal{J} = 10\log_{10}N_{\mathcal{J}}, \tag{B1}$$

where $N_{\mathcal{J}} = \ln\mathcal{J} = L_{\mathcal{J}}/(10\log_{10}e)$. The moment generating function for $N_{\mathcal{J}}$ is

$$M_{N_{\mathcal{J}}}(s) = E[e^{sN_{\mathcal{J}}}] \tag{B2}$$

$$= E[\mathcal{J}^s] \tag{B3}$$

$$= \frac{d^s}{du^s}M_{\mathcal{J}}(u)\Big|_{u=0}, \tag{B4}$$

where $M_{\mathcal{J}}(u)$ is the moment generating function of the Gamma distributed bandwidth averaged energy spectral density $\mathcal{J}$ with shape parameter μ_F and scale parameter $\bar{\mathcal{E}}/\mu_F$, given by

$$M_{\mathcal{J}}(u) = E[e^{u\mathcal{J}}] \tag{B5}$$

$$= \left[1-\frac{\bar{\mathcal{E}}}{\mu_F}u\right]^{-\mu_F}. \tag{B6}$$

The sth order derivative of $M_{\mathcal{J}}(u)$ is

$$M_{N_{\mathcal{J}}}(s) = \frac{d^s}{du^s}M_{\mathcal{J}}(u)\Big|_{u=0} \tag{B7}$$

$$= \frac{\Gamma(\mu_F+s)}{\Gamma(\mu_F)}\left(\frac{\bar{\mathcal{E}}}{\mu_F}\right)^s. \tag{B8}$$

The mean of $N_{\mathcal{J}}$ can be found from

$$\langle N_{\mathcal{J}}\rangle = \frac{d}{ds}M_{N_{\mathcal{J}}}(s)\Big|_{s=0} \tag{B9}$$

$$= \ln\bar{\mathcal{E}} - \ln\mu_F + \psi(\mu_F), \tag{B10}$$

where $\psi(\mu_F)$ is the Digamma function, written in its derivative and series forms as[36]

$$\psi(\mu_F) = \frac{1}{\Gamma(\mu_F)}\frac{d}{d\mu_F}\Gamma(\mu_F) \tag{B11}$$

$$= -\gamma + \sum_{k=0}^{\infty}\left(\frac{1}{k+1} - \frac{1}{k+\mu_F}\right), \tag{B12}$$

with $\gamma \simeq 0.57721\ldots$ being the Euler's constant.

The second moment of $N_{\mathcal{J}}$ is

$$\langle N_{\mathcal{J}}^2\rangle = \frac{d^2}{ds^2}M_{N_{\mathcal{J}}}(s)\Big|_{s=0} \tag{B13}$$

$$= \frac{1}{\Gamma(\mu_F)}\left\{\frac{d^2}{ds^2}\Gamma(\mu_F+s) + 2\ln(\bar{\mathcal{E}}/\mu_F)\frac{d}{ds}\Gamma(\mu_F+s) + [\ln(\bar{\mathcal{E}}/\mu_F)]^2\Gamma(\mu_F)\right\}\Big|_{s=0}. \tag{B14}$$

The derivative operator can now be performed on μ_F instead of s because for any function g defined at μ_F

$$\frac{d}{ds}g(\mu_F+s)\Big|_{s=0} = \lim_{\Delta s\to 0}\frac{g(\mu_F+\Delta s) - g(\mu_F)}{\Delta s} \tag{B15}$$

$$= \lim_{\Delta\mu_F\to 0}\frac{g(\mu_F+\Delta\mu_F) - g(\mu_F)}{\Delta\mu_F} \tag{B16}$$

$$= \frac{d}{d\mu_F}g(\mu_F). \tag{B17}$$

This also holds for the second derivative, which enables the second moment of $N_{\mathcal{J}}$ expressed in Eq. (B14) to be written as

$$\langle N_{\mathcal{J}}^2\rangle = \frac{d}{d\mu_F}\psi(\mu_F) + [\psi(\mu_F) + \ln\bar{\mathcal{E}} - \ln\mu_F]^2. \tag{B18}$$

Substituting the series form of the Digamma function given in Eq. (B12)–(B18), we find the standard deviation of $N_{\mathcal{J}}$ is

$$\sigma_{N_{\mathcal{J}}} = \sqrt{\langle N_{\mathcal{J}}^2\rangle - \langle N_{\mathcal{J}}\rangle^2}$$

$$= \sqrt{\frac{d}{d\mu_F}\left[-\gamma + \sum_{k=0}^{\infty}\left(\frac{1}{k+1} - \frac{1}{k+\mu_F}\right)\right]} \tag{B19}$$

$$= \sqrt{\sum_{k=0}^{\infty}\frac{1}{(k+\mu_F)^2}} \tag{B20}$$

$$= \sqrt{\zeta(2,\mu_F)}, \tag{B21}$$

where $\zeta(\nu,\ \mu_F)$ is the Riemann zeta function defined by

$$\zeta(\nu,\mu_F) = \sum_{k=0}^{\infty}\frac{1}{(k+\mu_F)^{\nu}}. \tag{B22}$$

The mean and standard deviation of $L_{\mathcal{J}}$ can now be obtained, respectively, as

$$\langle L_{\mathcal{J}}\rangle = 10\log_{10}(\bar{\mathcal{E}}/\mu_F) + (10\log_{10}e)\frac{\Gamma'(\mu_F)}{\Gamma(\mu_F)}, \tag{B23}$$

$$\sigma_{L_{\mathcal{J}}} = 10\log_{10}e\sqrt{\zeta(2,\mu_F)}. \tag{B24}$$

[1]J. W. Goodman, *Statistical Optics* (Wiley, New York, 1985), pp. 60–285.
[2]N. C. Makris, "The effect of saturated transmission scintillation on ocean acoustic intensity measurements," J. Acoust. Soc. Am. **100**, 769–783 (1996).
[3]L. Mandel and E. Wolf, *Optical Coherence and Quantum Optics* (Cambridge University Press, 1995), pp. 1–1164.
[4]G. J. Troup and R. G. Turner, "Optical coherence theory," Rep. Prog. Phys. **37**, 771 (1974).
[5]N. C. Makris, P. Ratilal, S. Jagannathan, Z. Gong, M. Andrews, I. Bertsatos, O. Godo, R. Nero, and J. M. Jech, "Critical population density triggers rapid formation of vast oceanic fish shoals," Science **323**, 1734–1737 (2009).
[6]Z. Gong, M. Andrews, S. Jagannathan, R. Patel, J. Jech, N. C. Makris, and P. Ratilal, "Low-frequency target strength and abundance of shoaling Atlantic herring (Clupea harengus) in the Gulf of Maine during the Ocean Acoustic Waveguide Remote Sensing 2006 Experiment," J. Acoust. Soc. Am. **127**, 104–123 (2010).
[7]P. R. Worcester, G. O. Williams, and S. M. Flatté, "Fluctuations of resolved acoustic multipaths at short range in the ocean," J. Acoust. Soc. Am. **70**, 825–840 (1981).
[8]S. M. Flatté, *Sound Transmission Through a Fluctuating Ocean* (Cambridge University Press, New York, 1979), pp. 1–305.
[9]J. Apel, M. Badiey, C.-S. Chiu, S. Finette, R. Headrick, J. Kemp, J. F. Lynch, A. Hewhall, M. Orr, B. H. Pasewark, D. Tielbbuerger, A. Turgut, K. von der Heydt, and S. Wolf, "An overview of the 1995 SWARM shallow-water internal wave acoustic scattering experiment," IEEE J. Ocean. Eng. **22**, 465–500 (1997).
[10]P. G. Bergmann, *Physics of Sound in the Sea* (Research Analysis Group, Washington, DC, 1946), pp. 158–172.
[11]I. Dyer, "Statistics of sound propagation in the ocean," J. Acoust. Soc. Am. **48**, 337–345 (1970).
[12]P. N. Mikhalevsky, "Envelope statistics of partially saturated processes," J. Acoust. Soc. Am. **72**, 151–158 (1982).
[13]A. Leon-Garcia, *Probability and Random Processes for Electrical Engineering* (Addison-Wesley, Reading, MA, 1994), pp. 116–150.
[14]T. E. Ewart, "A model of the intensity probability distribution for wave propagation in random media," J. Acoust. Soc. Am. **86**, 1490–1498 (1989).
[15]A. Fredricks, J. A. Colosi, J. F. Lynch, G. Gawarkiewicz, C.-S. Chiu, and P. Abbot, "Analysis of multipath scintillations from long range acoustic transmissions on the New England continental slope and shelf," J. Acoust. Soc. Am. **117**, 1038–1057 (2005).
[16]M. Andrews, T. Chen, and P. Ratilal, "Empirical dependence of acoustic transmission scintillation statistics on bandwidth, frequency, and range in New Jersey continental shelf," J. Acoust. Soc. Am. **125**, 111–124 (2009).
[17]J. A. Colosi, E. K. Scheer, S. M. Flatté, B. D. Cornuelle, M. A. Dzieciuch, W. H. Munk, P. F. Worcester, B. M. Hower, J. A. Mercer, R. C. Spindel, K. Mertzger, T. G. Birdsall, and A. B. Baggeroer, "Comparisons of measured and predicted acoustic fluctuations for a 3250-km propagation experiment in the eastern north pacific ocean," J. Acoust. Soc. Am. **105**, 3202–3218 (1999).
[18]R. Headrick, J. F. Lynch, J. Kemp, A. Newhall, K. von der Heydt, J. R. Apel, M. Badiey, C.-S. Chiu, S. Finette, M. H. Orr, B. H. Pasewark, A. Turgut, S. Wolf, and D. Tielbuerger, "Acoustic normal-mode fluctuation statistics in the 1995 SWARM internal wave scattering experiment," J. Acoust. Soc. Am. **107**, 201–220 (2000).
[19]C.-S. Chiu, S. R. Ramp, C. W. Miller, J. F. Lynch, T. F. Duda, and T. Y. Tang, "Acoustic intensity fluctuations induced by South China Sea internal tides and solitons," IEEE J. Ocean. Eng. **29**, 1249–1263 (2005).
[20]J. A. Colosi, A. B. Baggeroer, B. D. Cornuelle, M. A. Dzieciuch, W. H. Munk, P. F. Worcester, B. D. Dushaw, B. M. Howe, J. A. Mercer, R. C. Spindel, T. G. Birdsall, K. Metzger, and A. M. G. Forbes, "Analysis of multipath acoustic field variability and coherence in the finale of broadband basin-scale transmissions in the North Pacific Ocean," J. Acoust. Soc. Am **117**, 1538–1564 (2005).

[21]N. C. Makris, P. Ratilal, D. T. Symonds, S. Jagannathan, S. Lee, and R. W. Nero, "Fish population and behavior revealed by instantaneous continental shelf-scale imaging," Science **311**, 660–663 (2006).
[22]J. R. Preston, T. K. Akal, and J. M. Berkson, "Analysis of backscattering data in the Tyrrhenian sea," J. Acoust. Soc. Am. **87**, 119–134 (1990).
[23]R. J. Urick, *Principles of Underwater Sound* (McGraw-Hill, New York, 1983), pp. 1–406.
[24]T. M. Cover and J. A. Thomas, *Elements of Information Theory* (Wiley, New York, 2006), pp. 183–240.
[25]J. G. Proakis, E. M. Sozer, J. A. Rice, and M. Stojanovic, "Shallow water acoustic networks," IEEE. Commun. Mag. **39**, 114–119 (2001).
[26]D. H. Cato, "Simple methods of estimating source levels and locations of marine animal sounds," J. Acoust. Soc. Am. **104**, 1667–1678 (1998).
[27]A. M. Thode, G. L. D'Spain, and W. A. Kuperman, "Matched-field processing, geoacoustic inversion, and source signature recovery of blue whale vocalizations," J. Acoust. Soc. Am. **107**, 1286–1300 (2000).
[28]W. W. L. Au, A. A. Pack, M. O. Lammers, L. M. Herman, M. H. Deakos, and K. Andrews, "Acoustic properties of humpback whale songs," J. Acoust. Soc. Am. **120**, 1103–1110 (2000).
[29]G. E. Stanford, "Low-frequency fluctuations of a CW signal in the ocean," J. Acoust. Soc. Am. **55**, 968–977 (1974).
[30]T. C. Yang, "Measurements of temporal coherence of sound transmissions through shallow water," J. Acoust. Soc. Am. **120**, 2595–2614 (2006).
[31]K. Becker and J. R. Preston, "The ONR Five Octave Research Array (FORA) at Penn State," IEEE J. Ocean. Eng. **5**, 2607–2610 (2003).
[32]T. Chen, P. Ratilal, and N. Makris, "Temporal coherence after multiple forward scattering through random three-dimensional inhomogeneities in an ocean waveguide," J. Acoust. Soc. Am. **124**, 2812–2822 (2008).
[33]R. E. Williams and H. F. Battestin, "Time coherence of acoustic signals transmitted over resolved paths in the deep ocean," J. Acoust. Soc. Am. **59**, 312–328 (1976).
[34]M. D. Collins, "Generalization of the split-step Padé solution," J. Acoust. Soc. Am. **96**, 382–385 (1994).
[35]J. A. Colosi and A. B. Baggeroer, "On the kinematics of broadband multipath scintillation and the approach to saturation," J. Acoust. Soc. Am **116**, 3515–3522 (2004).
[36]M. Abramowitz and I. A. Stegun, editors, *Handbook of Mathematical Functions with Formulas, Graphs, and Mathematical Tables* (Dover, New York, 1972), pp. 258–259.